A graded resonator array for amplification of water waves

M. A. Peter[1], **L. G. Bennetts**[2] **and R. V. Craster**[3]

[1]Institute of Mathematics, University of Augsburg, 86135 Augsburg, Germany
[2]School of Mathematical Sciences, University of Adelaide, Adelaide, SA 5005, Australia
[3]Department of Mathematics, Imperial College London, South Kensington Campus, UK
e-mail address: malte.peter@math.uni-augsburg.de

1 Introduction

At the workshop in Guidel-Plages in 2018, Peter *et al.* (2018) demonstrated rainbow trapping of water waves. Specifically, they showed how the energy of a normal incident wave can be amplified in truncated chirped crystals of rigid bottom-mounted cylinders, with lattice spacing increasing in the direction of the incident wave. The effect is due to the incident wave reaching a region inside the grating where its effective group velocity vanishes so that the incident energy accumulates. Different frequencies are amplified in different regions, leading to the phenomenon being referred to as rainbow trapping in the related literature, e.g. in acoustics. This idea could be used to increase the efficiency of power take-off devices in the ocean.

A drawback of the structure above is that it requires a considerable number of – albeit simple – members (some tens of cylinders) to be mounted in the ocean floor, which makes it rather expensive. Here, we expand on the idea of Peter *et al.* (2018) as in Bennetts *et al.* (2018) and present a related structure consisting of a much smaller number of members assembled in a single line. The chirping resonance effect is achieved by using C-shaped bottom-mounted cylinders, which provide a (leaky) internal resonance, as opposed to the full cylinders used previously. A much smaller number of cylinders suffices, and the amplification is even stronger than in the structure suggested before.

As a motivating example, Fig. 1 shows the depth-integrated wave energy, E, along a line array of ten C-shaped cylinders in a water domain of infinite horizontal extent ($x, y \in \mathbb{R}$), produced by plane incident waves travelling in the direction of the line (the x-direction, i.e. head-on incidence). Energy distributions are shown for five different wavelengths, λ, where the cylinder radius gradually increases from $3.25\,\mathrm{m}$ to $6.5\,\mathrm{m}$, and the incident energy is normalised to unity. To put the array dimensions in context, adjacent cylinder centres are $W = 15\,\mathrm{m}$ apart, which is less than three times smaller than the shortest wavelength considered, and means the overall length of the array is $142.75\,\mathrm{m}$, which is less than three times greater than the shortest wavelength and less than two times the longest wavelength.

The five incident wavelengths are chosen to be close to the longest-resonant wavelengths for cylinders 2, 4, 6, 8 and 10 (ordered from left to right). The maximum amplifications increase with increasing wavelength, from $E \approx 67.2$ in cylinder 1 for $\lambda = 49\,\mathrm{m}$, to $E \approx 524$ in cylinder 9 for $\lambda = 88\,\mathrm{m}$, which is over 11 times greater than the amplification for the cylinder in isolation. The amplifications have been attained without invoking optimisation strategies or parameter tuning.

2 Statement of the problem and solution method

We consider water-wave scattering by an arrangement of (non-overlapping) surface-piercing rigid bottom-mounted C-shaped cylinders in a domain of water of constant finite depth h and extending to infinity in all horizontal directions. Let the cylinders be indexed $m = 1, \ldots, M$ from left to right, and the domain occupied by the mth cylinder be $\mathcal{C}_m \times (-h, 0)$, where

$$\mathcal{C}_m = \{\mathbf{x} : (x - x_m, y) = a_m(\cos\vartheta_m, \sin\vartheta_m), \text{ where } \varphi - \pi < \vartheta_m < \pi - \varphi\}. \tag{1}$$
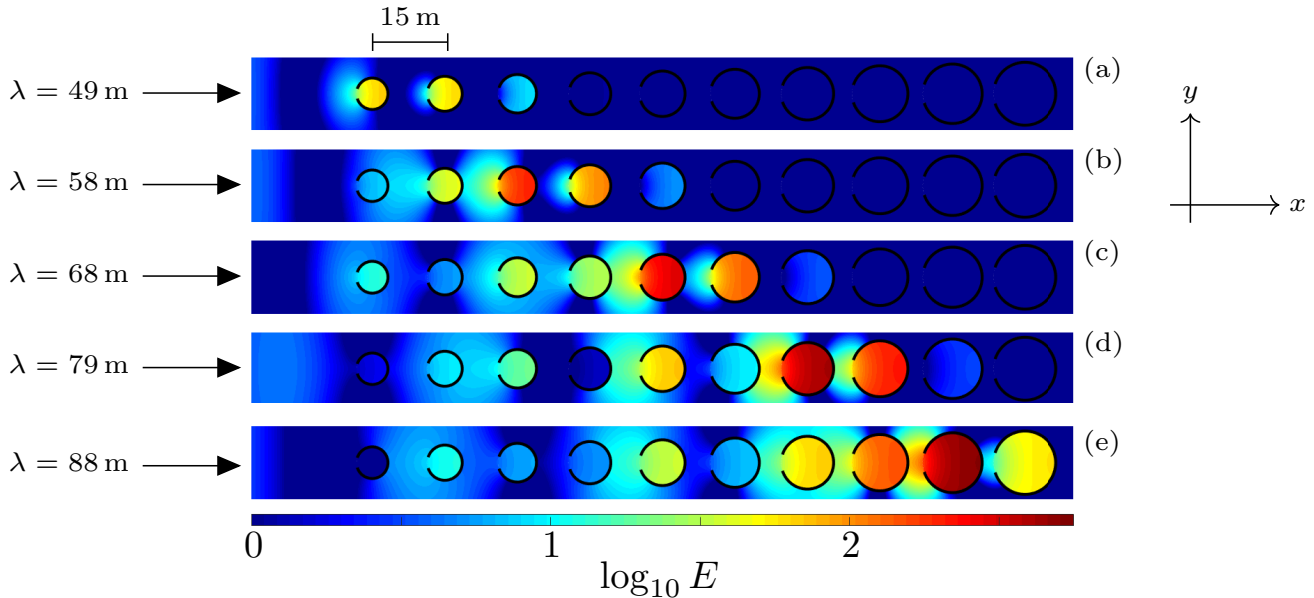
Figure 1: Logarithm of normalised energy along an array of ten C-shaped cylinders for head-on incident waves (propagating in the positive x-direction) with wavelengths (a) $\lambda = 49$ m, (b) 58 m, (c) 68 m, (d) 79 m and (e) 88 m, corresponding to resonant wavelengths in cylinder 2, 4, 6, 8 and 10, respectively (ordered left to right), when in isolation.

Here, $x_m = (m-1)W$ is the cylinder centre location along the x-axis, a_m is its radius, and φ is the half-angle of its opening (identical for all cylinders), and the openings are at the left-hand end of the cylinders and symmetric about the x-axis, as shown in Fig. 1.

The equations of motion for the water are derived from the linearised inviscid theory assuming irrotational motion. Restricting to time-harmonic motion with radian frequency ω, the velocity field is expressed as $\mathbf{u}(\mathbf{y},t) = \mathbb{Re}\left\{(gA/\mathrm{i}\omega)\nabla\phi(\mathbf{y})\mathrm{e}^{-\mathrm{i}\omega t}\right\}$, where $\mathbf{y} = (x,y,z)$ denotes a point in the water and ϕ is a (dimensionless) reduced complex-valued velocity potential. Moreover, A is the incident wave amplitude and $g \approx 9.81\,\mathrm{m\,s^{-2}}$ is the acceleration due to gravity. In what follows, the notation $\mathbf{x} = (x,y)$ denotes a point on the undisturbed water surface, assumed at $z = 0$, i.e. $\mathbf{x} = (x,y,0)$.

Writing $\alpha = \omega^2/g$, the potential ϕ has to satisfy the standard boundary-value problem

$$-\Delta\phi = 0, \ \mathbf{y} \in \mathcal{D}; \quad \frac{\partial\phi}{\partial z} = \alpha\phi, \ \mathbf{x} \in \Gamma^{\mathrm{f}}; \quad \frac{\partial\phi}{\partial z} = 0, \ \mathbf{y} \in \mathcal{D}, \ z = -h, \tag{2}$$

where $\Gamma^{\mathrm{f}} = \mathbb{R}^2\backslash\bigcup_j \overline{\mathcal{C}_j}$ is the free water surface and $\mathcal{D} = \Gamma^{\mathrm{f}} \times (-h,0)$ is the domain occupied by the water. The normal derivative of the potential on the cylinder surfaces is required to vanish, together with a condition ensuring the correct singularity at the tips of the C-shapes. Moreover, the Sommerfeld radiation condition is imposed in the far field. Owing to the constant cross-section of the cylinders, the depth dependence can be factored out of the problem. The potential can be solved for efficiently using a modified version of the recursive algorithm developed by Montiel *et al.* (2016) and Bennetts *et al.* (2017).

3 The role of Rayleigh–Bloch waves

Fig. 2 shows results that provide insights into the large amplifications observed in Fig. 1, for which the array is defined by $M = 10$, $W = 15$ m, $\varphi = 0.1\,\pi$, and $a_m = a_1(m + M - 2)/(M - 1)$ where $a_1 = 3.25$ m. The largest amplification case from Fig. 1, with $\lambda = 88$ m, is chosen as an example, and Fig. 2a is a magnified version of Fig. 1e.

As shown by Thompson *et al.* (2008) and others for uniform line arrays of ordinary cylinders (with $\varphi = 0$, i.e. full cylinders of circular cross-section), the scattered wave field along the array is
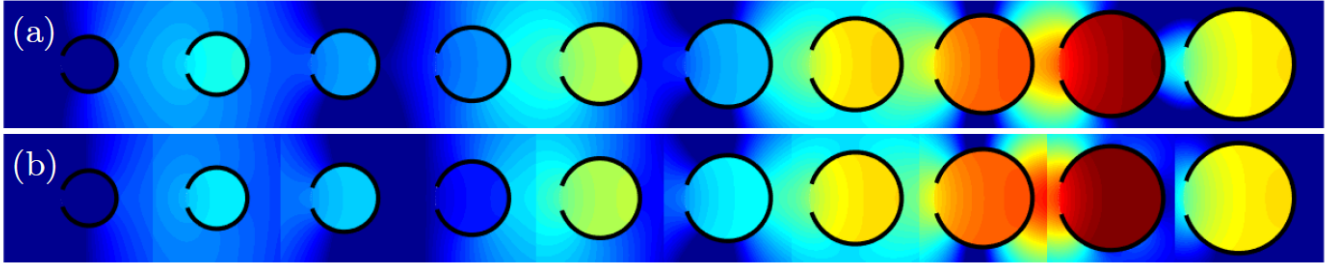
Figure 2: (a) Log of normalised energy as in Fig. 1e. (b) Corresponding energy with scattered wave field approximated by the local Rayleigh–Bloch-wave components only.

dominated by Rayleigh–Bloch waves, which propagate in both directions along the array and decay exponentially in the transverse direction (i.e. y-direction) away from it. Line arrays of C-shaped cylinders also support Rayleigh–Bloch waves (a new finding to our knowledge!), and the radius grading causes their properties to evolve along the array. Fig. 2b is similar to Fig 2a, but with the scattered wave field approximated by the Rayleigh–Bloch wave components only. The approximation is based on projecting the scattered wave field in each subinterval onto the eigenfunctions defined by the corresponding transfer matrix, and retaining only the eigenfunctions associated to *local* Rayleigh–Bloch waves, i.e. Rayleigh–Bloch waves associated to a particular cylinder and spacing. Notwithstanding the small discontinuities, which are an inevitable consequence of the approximation method, the approximation is highly accurate, particularly with respect to the large amplifications, thus confirming the amplifications are due to excitation of local Rayleigh–Bloch waves.

4   Amplification spectra

Fig. 3 quantifies the overall energy amplification produced by the graded array over ranges of incident wavelengths λ and directions ψ (the angle between the direction of propagation of the incident wave and the x-axis), using metrics analogous to the Q-factor familiar in assessing energy gains (or losses) given by arrays of interacting wave-energy converters (Falnes, 1980). Fig. 3a shows $\mathcal{Q}_{\mathrm{arr}} = \mathcal{E}/\mathcal{E}_{\mathrm{inc}}$ on a logarithmic scale, where $\mathcal{E} = \sum_{m=1}^{M} \int_{\Omega_m} |\phi|^2 \, \mathrm{d}\mathbf{x}$ and $\mathcal{E}_{\mathrm{inc}} = \sum_{m=1}^{M} \int_{\Omega_m} |\phi_{\mathrm{inc}}|^2 \, \mathrm{d}\mathbf{x} = \sum_{m=1}^{M} \pi a_m^2$ are, respectively, the scaled energy contained with the C-shaped cylinders along the array and the energy of the incident field over the same area. Here, $\Omega_m = \{\mathbf{x} : (x - x_m)^2 + y^2 < a_m\}$. Therefore, $\mathcal{Q}_{\mathrm{arr}}$ quantifies the overall amplification given by the array.

For head-on incidence, $\psi = 0$, the array amplifies the incident energy by over an order of magnitude for wavelengths $\lambda \in (60\,\mathrm{m}, 98\,\mathrm{m})$, with maximum amplification $\mathcal{Q}_{\mathrm{arr}} \approx 10^{1.53} \approx 33.6$. For wavelengths $\lambda < 60\,\mathrm{m}$, the amplification reduces as wavelength decreases, due to the associated frequencies lying in quasi-bandgaps for the cylinders at the leading end of the array, so that only small quantities of wave energy penetrate the array. For wavelengths shorter than those shown, higher-order resonances alter this simple trend. For wavelengths $\lambda > 98\,\mathrm{m}$, the amplification asymptotes towards unity as the influence of the cylinder on the waves reduces. The behaviour is similar for non-head-on incidence, with some reduction in amplification, as Rayleigh–Bloch waves are not as strongly excited due to the loss of symmetry in the incident field with respect to the axis of the array. Amplifications of over an order of magnitude exist up to $\psi \approx 0.18\,\pi$, and the wavelength interval for which the amplification is over an order of magnitude is at least $25\,\mathrm{m}$ long up to $\psi = 0.15\,\pi$.

Fig. 3b shows $\mathcal{Q}_{\mathrm{grd}} = \mathcal{E}/\mathcal{E}_0$ on a logarithmic scale, where $\mathcal{E}_0 = \sum_{m=1}^{M} \int_{\Omega_m} |\phi_m|^2 \, \mathrm{d}\mathbf{x}$, with ϕ_m the velocity potential for the mth cylinder in isolation, i.e. with no surrounding cylinders. Therefore, $\mathcal{Q}_{\mathrm{grd}}$ quantifies the overall energy amplification given by the radius grading, independent of the amplification due to the cylinder resonances. As indicated by Figs. 1–2, for head-on incidence the grading is most effective for wavelengths that excite resonances in the cylinders towards the trailing end of the array. The maximum overall amplification due to grading is $\mathcal{Q}_{\mathrm{grd}} \approx 10^{0.77} \approx 5.87$ for
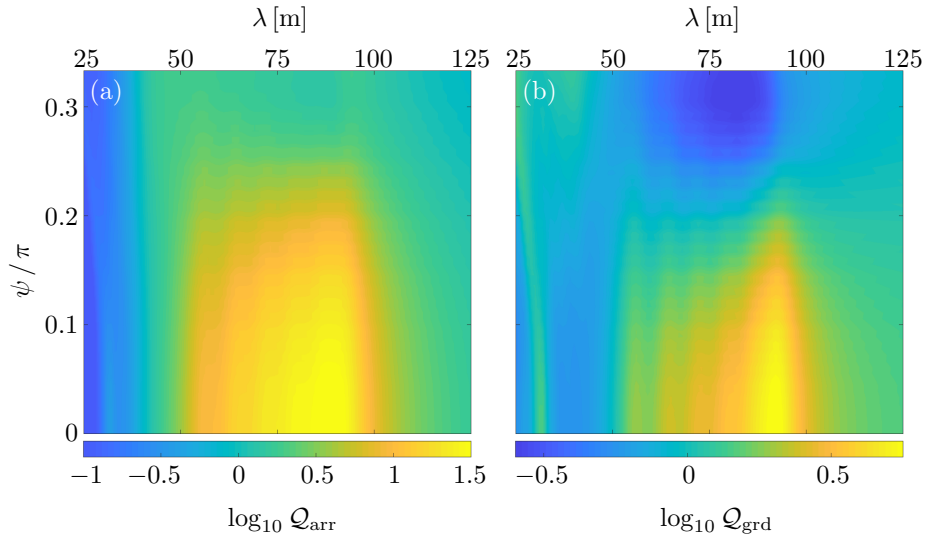
Figure 3: Logarithmic Q-factors as functions of incident wavelength and direction. (a) $\mathcal{Q}_{\mathrm{arr}} = \mathcal{E}\,/\,\mathcal{E}_{\mathrm{inc}}$, where $\mathcal{E}$ is the integrated energy within the C-shaped cylinders along the array, and $\mathcal{E}_{\mathrm{inc}}$ is the incident energy over the same domain. (b) $\mathcal{Q}_{\mathrm{grd}} = \mathcal{E}\,/\,\mathcal{E}_0$, where $\mathcal{E}_0$ is the integrated energy within equivalent isolated C-shaped cylinders.

$\lambda \approx 92\,\mathrm{m}$. The amplification is positive for $\lambda > 50\,\mathrm{m}$, with negative amplifications associated to quasi-bandgaps for shorter waves, as noted above. Similarly, the strength of amplification due to grading slowly decreases as the incident wave direction moves away from head-on incidence, with the grading more than trebling the overall amplification, i.e. $\mathcal{Q}_{\mathrm{grd}} > 3$, for wavelengths around $\lambda = 92\,\mathrm{m}$ up to $\psi \approx 0.15\,\pi$.

5   Conclusions

A graded line array of C-shaped cylinders has been proposed as a structure for frequency separation and amplification of water-wave energy, and with structural dimensions comparable to the target wavelengths. Using linear potential-flow theory, and an example in which the array consists of ten cylinders with graded radii, it was shown that the resonant amplifications within a given cylinder in the array far exceed those of the cylinder in isolation, and that typically even larger amplifications occur in the preceding cylinder. Further, the array was shown to be effective in terms of the overall amplification, over broad ranges of wavelengths and incident directions.

References

BENNETTS, L. G., PETER, M. A. & CRASTER, R. V. 2018 Graded resonator arrays for spatial frequency separation and amplification of water waves. *J. Fluid Mech.* **854**, R4.

BENNETTS, L. G., PETER, M. A. & MONTIEL, F. 2017 Localisation of Rayleigh–Bloch waves and damping of resonant loads on arrays of vertical cylinders. *J. Fluid Mech.* **813**, 508–527.

FALNES, J. 1980 Radiation impedance matrix and optimum power absorption for interacting oscillators in surface waves. *Appl. Ocean Res.* **2** (2), 75–80.

MONTIEL, F., SQUIRE, V. A. & BENNETTS, L. G. 2016 Attenuation and directional spreading of ocean wave spectra in the marginal ice zone. *J. Fluid Mech.* **790**, 492–522.

PETER, M. A., BENNETTS, L. G. & CRASTER, R. V. 2018 Rainbow trapping of water waves. In *Proc. 33rd Int. Workshop on Water Waves and Floating Bodies, Guidel-Plages, France* (ed. Y.-M. Scolan), pp. 157–160.

THOMPSON, I., LINTON, C. M. & PORTER, R. 2008 A new approximation method for scattering by long finite arrays. *Q. J. Mech. Appl. Math.* **61** (3), 333–352.